Phase transitions in a three-dimensional Ising model with cluster weight studied by Monte Carlo simulations

Ziyang Wang,[1,2] Le Feng,[2] Wanzhou Zhang,[1,2,*] and Chengxiang Ding[3,†]

[1]*Key Laboratory of Quantum Information, University of Science and Technology of China, Chinese Academy of Sciences, Hefei 230026, People's Republic of China*

[2]*College of Physics and Optoelectronics, Taiyuan University of Technology, Shanxi 030024, China*

[3]*School of Science and Engineering of Mathematics and Physics, Anhui University of Technology, Maanshan 243002, China*

(Received 22 July 2021; accepted 14 September 2021; published 22 October 2021)

The loop model is an important model of statistical mechanics and has been extensively studied in two-dimensional lattices. However, it is still difficult to simulate the loop model directly in three-dimensional lattices, especially in lattices with coordination numbers larger than 3. In this paper, a cluster weight Ising model is proposed by introducing an additional cluster weight n in the partition function of the traditional Ising model. This model is equivalent to the loop model on the two-dimensional lattice, but on the three-dimensional lattice, it is still not very clear whether or not these models have the same universality. By using a Monte Carlo method with cluster updates and color assignment, we obtain the global phase diagram containing the paramagnetic and ferromagnetic phases. The phase transition between the two phases is second order at $1 \leqslant n < n_{cri}$ and first order at $n \geqslant n_{cri}$, where $n_{cri} \approx 2$. The thermal exponent y_t is equal to the system dimension d when the first-order transition occurs. For the second-order transitions, the numerical estimation of y_t and the magnetic exponent y_m, shows that the universalities of the two models on the three-dimensional lattice are different. Our results are helpful in the understanding of some traditional statistical mechanics models.

DOI: 10.1103/PhysRevE.104.044132

I. INTRODUCTION

A basic task in statistical physics is revealing the universalities of many theoretical models describing the common properties of different kinds of materials. The the earliest standard model in statistical physics is the Ising model, proposed by Ising in 1925 [1]. The model was generalized to a large variety of models, such as the $O(n)$ spin model initially defined by Stanley [2] as n-component spins interacting in an isotropic way. Another interesting model is the n-component face cubic model, which is usually defined as a Hamiltonian containing two nearest-neighbor interactions between n-component spins that point to the faces of an n-dimensional hypercube [3,4]. The face cubic model's counterpart is a corner cubic model with spins pointing to the corners instead of faces of the hypercube [4,5].

The critical properties of the $O(n)$ spin model and n-component face cubic model have been studied and compared extensively in the language of graphs by expanding the partition function in powers of the interaction strength between spins and integrating the spin variables. The $O(n)$ spin model should be able to be mapped to the loop model [6–9], where the parameter n is not restricted to integers. Similarly, mappings exist ranging from the n-component face cubic model to the so-called cubic loop model as named in Ref. [10] or the Eulerian bond-cubic model [11,12], as each vertex (site) connects an even number of bonds. On the square lattice, in the range $1 \leqslant n < 2$, the $O(n)$ loop model and n-component face cubic model [11] belong to the same universality class, and the critical exponents are expected to be obtained by mapping the model to the Coulomb gas model [13]. The differences between the two models start at $n = 2$ because the $O(2)$ spin model undergoes a topological phase transition [14–16] while the n-component face cubic model undergoes a second-order transition [11]. For the $n > 2$ loop model on the honeycomb lattices, the phase transition belongs to the three-state Potts universality [17]. On the square lattices, the $n > 2$ loop model is of an Ising-like transition [8,18]. However, the $n > 2$ n-component face cubic loop model undergoes a first-order transition [19]. In three dimensions, the $O(n)$ symmetry can lead to continuous transitions at very large n [20,21], while the cubic symmetry makes the transition discontinuous in the range $n > n_{cri}$ with $n_{cri} \approx 2.89$ [22].

In order to access the rich critical properties of the loop model, the local updates of a Monte Carlo (MC) simulation is performed, although it is a difficult though interesting task due to the nonlocal weight in the partition sum of the model [9]. To solve this problem, a cluster algorithm combining the tricks of the Swendsen-Wang (SW) algorithm [23] and the "coloring method" was proposed by Deng *et al.* [24]. In this algorithm, the microstate (configuration) of the loop model is represented by the configuration of Ising spins, and the loops are regarded as the domain walls [9,25] of the Ising clusters. However, a problem arises naturally. Such a representation is applicable only in two-dimensional honeycomb lattices because there is no loop intersection phenomenon. In three dimensions with

*Corresponding author: zhangwanzhou@tyut.edu.cn

†Corresponding author: dingcx@ahut.edu.cn

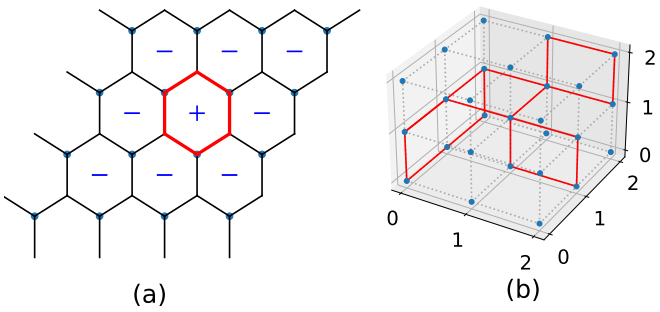

FIG. 1. (a) On a honeycomb lattice, the loop marked in red is just the domain walls of the Ising clusters. There is a total of $n_c = 2$ clusters and $l = 1$ loop. (b) On a cubic lattice, the graph may not satisfy the planarity, required by the relationship $n_c = l + 1$.

a maximum coordination number of 3 due to the special topology, the loop model was simulated by resorting to other methods, such as the worm algorithm [26,27].

In this paper we pay special attention to the Ising representation. In fact, the two-dimensional loop model can be regarded as an Ising model with cluster weight, which we will explain in detail in the next section. A generalization of such a "cluster-weighted Ising" (CWI) model to three-dimensional lattice is applicable and straightforward, and the cluster algorithm is still applicable for it. We investigate this model with MC simulations and compare its critical properties with the results from the loop models [11,21].

The outline of this work is as follows. Section II introduces the loop model and its Ising representation on the honeycomb and cubic lattices, the proposed CWI model. The difficulty of simulating the loop model in nonplanar graphs is also described. Section III describes the cluster update algorithm and several sampled observables in MC simulations. Numerical results are then presented in Sec. IV. The global phase diagram is shown, and the critical exponents for the first- and second-order transitions are presented. The efficiency of the algorithm and how to get the error bars are also discussed. Concluding comments are made in Sec. V.

II. ISING MODEL WITH A CLUSTER WEIGHT

We start with the partition function of the loop model,

$$Z_{\text{loop}} = \sum_{\{G\}} x^b n^l, \tag{1}$$

where l, n, b are the number of loops, weight of each loop, and weight of each bond, respectively. The symbol G means all possible configurations of loops. The loop configuration on the honeycomb lattice can be represented by the Ising configuration on the triangular lattice (dual lattice of the honeycomb lattice), and the loops are just the domain walls [9,25] of the Ising clusters. The number of the Ising clusters n_c is just the number of loops l plus 1, namely, $n_c = l + 1$. As shown in Fig. 1(a), two Ising clusters are separated by the red loop. It is important to note that for the honeycomb lattices, intersecting loops do not emerge. The reason for this is that each configuration is composed of an Eulerian bond graph where "Eulerian" means each site (vertex) is connected to an even number of bonds.

However, for the square lattice, similar to the cubic lattice shown in Fig. 1(b), loop intersecting will occur. This will cause difficulties in counting the number of loops during simulations. Not only a square lattice, but any lattices with degree more than 3 will cause such confusion. Namely, each site connects more than three sites.

One way to solve this issue is to avoid using the term "number of loops" in Eq. (1) because such a quantity is not well defined on graphs with degree above 3. The correct term is "cyclomatic number," defined to be the minimum number of edges required to be deleted from a graph in order to obtain a forest [28]. The value of the "cyclomatic number" is $l = e - n_s + 1$, where e and n_s are the numbers of bonds and the sites in the lattices, respectively. On graphs of maximum degree 3, the cyclomatic number does indeed count the number of loops l.

On the other hand, when considering the definition of "cyclomatic number" l, the relation $n_c = l + 1$ still holds for the square and honeycomb lattices, but this is true only for planar graphs. The requirement of planarity is very crucial. For the cubic lattices, the graph may not satisfy the requirement.

Here we propose to study directly the CWI model in the language of Ising clusters in the dual lattices rather than loop language. The partition function of the CWI model proposed reads as

$$Z_{\text{CWI}} = \sum_{\{S_i\}} \exp(-H) n^{n_c}, \tag{2}$$

with the reduced Hamiltonian of the well-known Ising model,

$$H = -K \sum_{\langle i,j \rangle} S_i S_j, \tag{3}$$

where $K = J/k_B T$. The term n^{n_c} is a factor of the cluster weight, and n is the weight of each cluster and is not limited to an integer. The clusters are formulated by the connected spins with same directions.

The exploration of the CWI model will help to understand the loop model. By doing similar work like the low-temperature expansion [29], the above model can be transformed into a loop model with the relation $x = \exp(-2K)$ between the parameters x and K. The study of the CWI model helps us understand the n-component face cubic model [10–12], whose partition function can be transformed into that similar to a loop model.

III. ALGORITHM AND OBSERVABLES

The algorithm to simulate this model is as follows:

(1) Initialize the randomly assigned configuration.

(2) Construct the Ising clusters: for a pair neighborhood sites i and j, if $S_i = S_j$, then absorb site j into the cluster.

(3) Assign each Ising cluster in green (active) a probability of $1/n$, but for a cluster in red (inactive) a probability of $1 - 1/n$.

(4) Construct the SW clusters: for the site i, add its neighborhood site j into the cluster according to the following rules:

(a) No matter what the of the spins on the sites i and j are, the only consideration is the color assigned the sites. If

one site in the site i and j is in red, then absorb the site j into the cluster absolutely.

(b) If both sites i and j are in green, then absorb site j into to the cluster with a probability of $p = 1 - e^{-2K}$ if $S_i = S_j$.

(5) Flip the clusters with a probability 1/2.

This algorithm is precisely introduced in Ref. [24]. In this paper, we apply it only to nonplanar graphs. Meanwhile, it would be worth mentioning that there is no particular reason to use the SW algorithm for the Ising updates on the active subgraph in step 4. Actually, "any" valid Ising MC method would suffice, such as the worm algorithm [30], the Sweeny algorithm [31], or the dynamic connectivity checking algorithm [32].

Considered that we assign the clusters red (inactive) with a probability of $1 - 1/n$, hence the algorithm we use works only for $n \geqslant 1$ even though the CWI model is well defined for any $n > 0$. With the help of the above algorithm, the sampled observables with magnetization m, magnetic susceptibility χ, specific heat C_V, and Binder ratio Q are defined as follows:

$$m = \langle |\mathcal{M}| \rangle, \tag{4}$$

$$Q = \langle \mathcal{M}^2 \rangle^2 / \langle \mathcal{M}^4 \rangle, \tag{5}$$

$$\chi = \frac{L^3}{k_B T} [\langle \mathcal{M}^2 \rangle - \langle \mathcal{M} \rangle^2], \tag{6}$$

$$C_V = \frac{1}{k_B T^2} [\langle E^2 \rangle - \langle E \rangle^2], \tag{7}$$

with $\mathcal{M}$ defined as

$$\mathcal{M} = \sum_i S_i / L^3. \tag{8}$$

These physical quantities have their scaling behavior as a function of the system size L and the thermodynamic temperature T:

$$m = L^{y_m - d} [m_0 + a_1 (T - T_c) L^{y_t} + a_2 (T - T_c)^2 L^{2y_t} + \cdots + b_1 L^{y_1} + b_2 L^{y_2} + \cdots], \tag{9}$$

$$Q = Q_0 + e_1 (T - T_c) L^{y_t} + e_2 (T - T_c)^2 L^{2y_t} + \cdots + f_1 L^{y_1} + f_2 L^{y_2} + \cdots, \tag{10}$$

where T_c is the critical temperature, y_t is the thermal exponent, y_m is the magnetic exponent, d is the space dimension, and y_1, y_2, …, are the negative correction-to-scaling exponents. The expansion coefficients a_i, b_i, e_i, f_i, $(i = 1, 2, \ldots)$ emerging in the two scaling functions are different in general.

The fitting function in Eq. (9) describes how m depends on the expansion coefficients, and at the critical points, the function is reduced to

$$m = L^{y_m - d} (m_0 + b_1 L^{y_1} + b_2 L^{y_2} + \cdots), \tag{11}$$

which is used to determine the exponent y_m.

IV. RESULTS

A. Global phase diagram and exponents

Figure 2 shows the global phase diagram containing, the paramagnetic (PM) and ferromagnetic (FM) phases, where

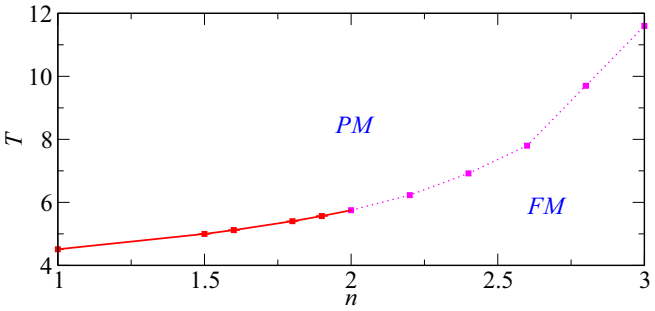

FIG. 2. The global phase diagram in the plane T vs n, containing the FM and PM phases. The dashed (solid) lines denote a first- (second-order) transition.

the dashed line denotes the first-order transition in the range $n_{cri} \leqslant n < 3$ and the solid line represents the second-order transition in the range $1 \leqslant n < n_{cri}$, where $n_{cri} \approx 2$.

For different values of n, the numerical exponents y_t and y_m at the critical points are listed in Table I. The numerical estimation of y_t and y_m is different from the values of the loop model [21] for $n = 1.5$. For $n = 2$, the value of the scaling dimension y_t is equal to the system dimension within error bars, which confirms that a first-order transition occurs between the PM and FM phases.

To summarize, for $n > 1$ on the 3D lattices, the universalities of the CWI model and the loop model are different.

The above conclusions are obtained via the MC simulations, and the details are as follows. The first 10^5–10^6 (MC) steps of simulation are performed in order to let the system reach equilibrium states. Then 10^5 samples in each thread (totally 100 threads) are taken to calculate each quantity for the system sizes $16 \leqslant L \leqslant 144$.

Typically, in the regimes of a continuous phase transition, taking $n = 1.5$ as an example, the dynamical exponent is estimated to be $z = 0.45(3)$ (see Sec. IV D). The autocorrelation time $\tau_{\text{int}} = L^z$, is sufficiently smaller than the number of samples. Therefore, there are enough independent samples between the total 10^7 samples.

As for other values of n, such as $n \geqslant 2$, it is still not easy to obtain the quantities z and τ_{int}. The reason for this is that the mixing time of the SW algorithm is slow and τ_{int} does not obey L^z when the first-order phase transition occurs [33]. However, we still use enough different samples to obtain convincing data and examine the conclusions in many different ways.

TABLE I. Comparison of the numerical exponents with those exponents of the loop model on three-dimensional lattices [21]. The critical temperature T_c, thermal exponent y_t, and magnetic exponent y_m for different values of n. The estimated errors in the last decimal place are shown in parentheses.

	CWI model			Loop model	
n	T_c	y_t	y_m	y_t	y_m
1.0	4.5115(1)	1.584(4)	2.487(1)	1.588(2)	2.483(3)
1.5	4.99912(5)	1.639(6)	2.400(5)	1.538(4)	2.482(3)
1.6	5.12147(5)	1.71(5)	2.34(2)	—	—
2.0	5.7514(2)	2.95(5)	—	1.488(3)	2.483(2)

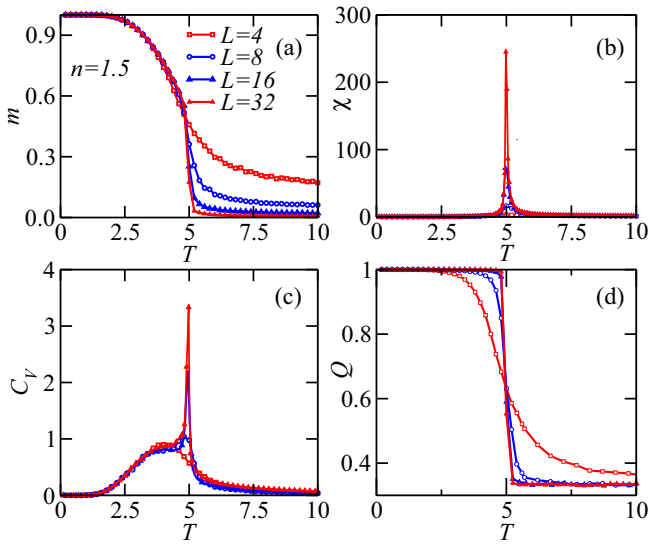

FIG. 3. (a) m, (b) χ, (c) C_V, (d) Q vs T at $n = 1.5$ in the range $0 < T < 10$, with different sizes $L = 4$, 8, 16, and 32, respectively. The peaks or jumps are located at the position $T_c \approx 5$.

For $n = 1$, the CWI model is reduced to the pure Ising model, which has been simulated in a higher precision according to Ref. [34]. The algorithm described previously reduces to the standard SW cluster algorithm [23]. Concurrently, the simulation and analysis of the $n = 1$ case are shown as benchmarks in the Appendix.

B. $n = 1.5$, detailed analysis

To get the regime of the critical point, we scan the temperature in the range $0 < T < 10$. In Fig. 3 the quantities m, χ, C_V, and Q are shown with different system sizes $L = 4$, 8, 16, and 32. From the position of peaks and jumps, T_c is around 5.

To obtain more accurate values of T_c, the Levenberg-Marquardt (LM) least-squares fit [35] of of Eq. (10) is performed, and the weighted distance between data points and fitting function is defined as $\Delta_i = Q(T_i; \{a_n\}) - Q_i$, where a_n is the parameter to be fitted including the exponents y_t, y_1, y_2, the coefficients e_1, e_2, f_1, f_2, and other quantities Q_0 and T_c. In practice, the error, i.e., standard deviation σ_i of the data points Q_i, is divided aiming to minimize the quadratic distance,

$$\chi^2 = \sum_{i=1}^{N} \frac{\Delta_i^2}{\sigma_i^2} = \sum_{i=1}^{N} \frac{[Q(T_i; \{a_n\}) - Q_i]^2}{\sigma_i^2}. \tag{12}$$

In Fig. 4(a) Q vs T is calculated in a very narrow region $4.9990 < T < 5.0002$ with many different sizes $L = 4$–112, and the precise critical point is found to be $T_c = 4.99912(5)$.

Correspondingly, the thermal exponent is estimated to be $y_t = 1.639(6)$. This value is obtained by calculating the average of y_t through different $L_{\min}$, and the different values of χ^2/dof are also shown in Fig. 4(b). The resulting y_t obtained is different from 1.538(4), which is the result from the loop model in Ref. [21].

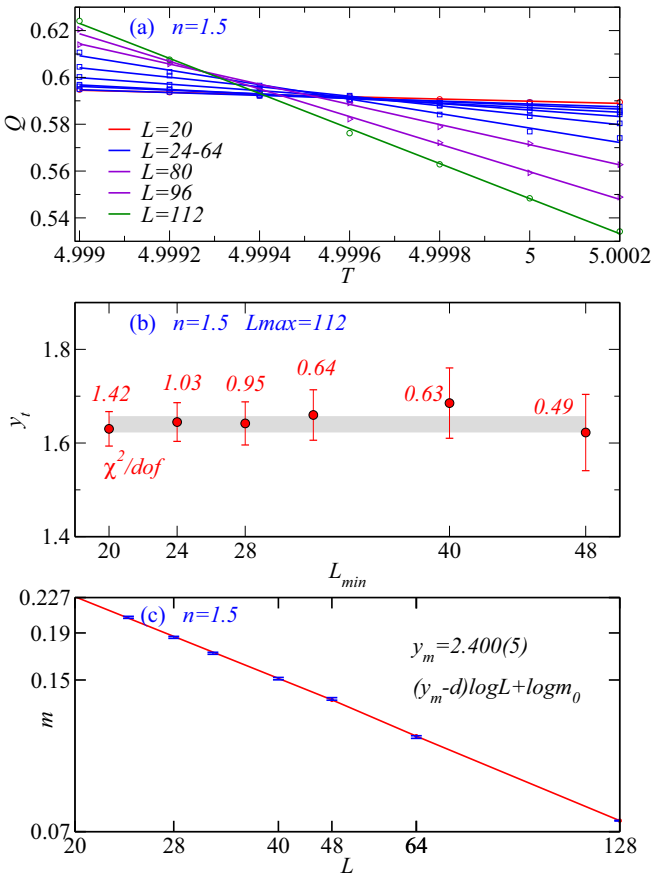

FIG. 4. (a) The Binder ratio Q vs T at $n = 1.5$ with different sizes. (b) y_t vs $L_{\min}$. The values of χ^2/dof are marked by the numbers in red. (c) The log-log plot of m vs L. A more accurate critical point is obtained at $T_c = 4.99912(5)$.

To get the magnetic exponent y_m, in Fig. 4(c) the log-log plot m vs system size L is shown and according to the equation

$$\log(m) = (y_m - d)\log(L) + \log(m_0) \tag{13}$$

or equivalently the power relationship $m = m_0 L^{y_m - d}$, which is the lead term of Eq. (11). The fitted exponent y_m is estimated to be 2.400(5) and is also different from 2.482(3) from the loop model in the last two significant digits.

The values of y_t and y_m mean that the CWI model is not in the same universality as the pure loop model.

C. $n = 2$, 3, a first-order phase transition

We gradually increase n in the range $2 \leqslant n < 3$. Since first-order transitions are difficult to study, we first consider simulating significantly larger n values, which should be safely done in the strongly first-order regime. The methods used involve plotting the histograms of the hysteresis and of m and E [36–38], and checking whether or not the exponent of y_t equals d. For $n = 2$, the histogram and fitting of Eq. (10) are used. The results by different methods are checked against each other.

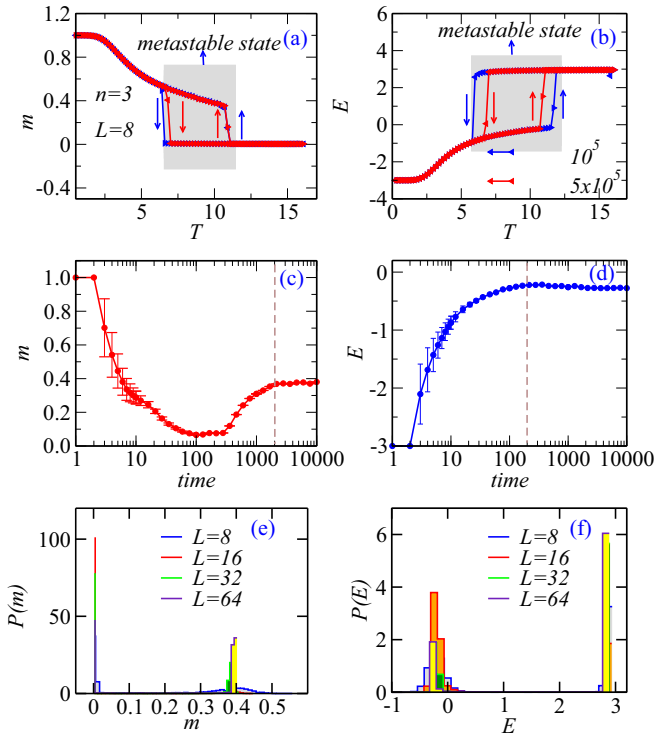

FIG. 5. (a) Hysteresis loop of the quantity m vs T; (b) the quantity E vs T; (c, d) m, E vs MC time at $T = 10$; (e, f) double-peak distributions of the histograms of m, E at $n = 3$, with different sizes $L = 8$, 16, 32, and 64.

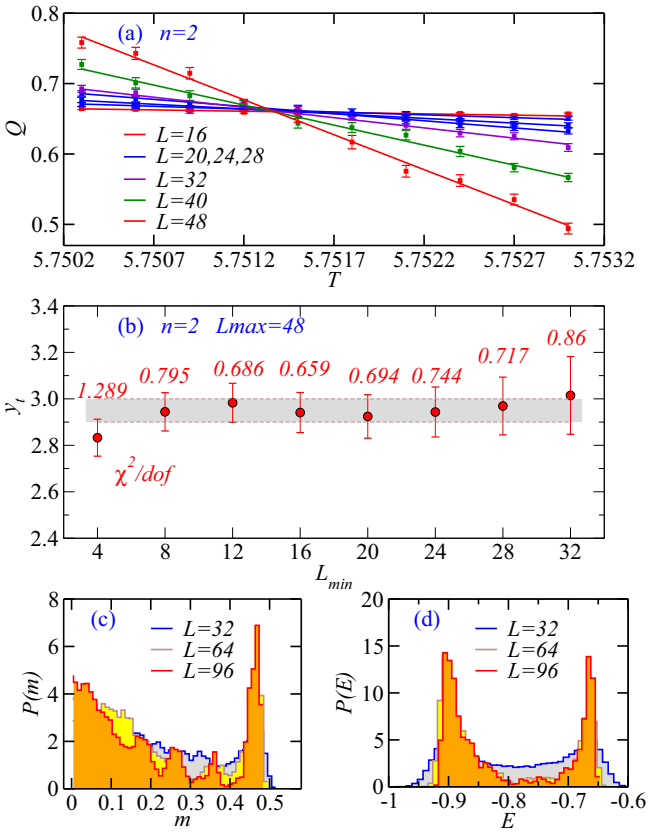

FIG. 6. (a) The Binder ratio Q vs T at $n = 2$ with different sizes; (b) y_t vs $L_{\min}$; (c) double-peak distributions of the histograms m at $n = 2$; (d) double-peak distributions of the histograms of E at $n = 2$ for $T = 5.755$, 5.7518, and 5.7516, respectively.

1. n = 3

To show the signature of a first-order transition for sufficiently large $n = 3$, we draw the hysteresis loops of the absolute magnetization m and energy E in Figs. 5(a) and 5(b) in the range $0 < T < 15$, respectively. The expression for the energy E is

$$E = \frac{\left[-J\sum_{\langle i,j\rangle} S_i S_j - n_c \log(n)\right]}{L^3}, \tag{14}$$

where n_c is the number of Ising clusters in a spin configuration. The hysteresis loops have been observed both in the classical Baxter-Wu model [39] and in the site random cluster model [40], as well as quantum systems [41–43], which means that there is obviously a first-order phase transition [44,45].

Although the SW algorithm has a global update advantage, it still has a slow mixing time for a first-order transition regime as proven in Ref. [33], which can be used to form a closed hysteresis loop. Initializing with the temperature $T = 0$, we increase T as well as sample the energy per site E. In the simulation of a given value of T, we treat the spin configuration of the completed simulation, as the (new) initial configuration of the simulation for the next value of T. After T exceeds T_c by a small value, the energy per site E jumps to a higher value. We decrease T in the same way with regard to the initialization of configurations. A closed hysteresis loop takes shape when T becomes smaller than T_c. We repeat these steps in a similar fashion for m, and the loop is shown in Fig. 5(b).

The hysteresis loops are caused by the fact that the lifetimes of the metastable states are much longer than the time intervals between temperature variations [39], and simulation and the measurements are taken from metastable states, marked by the gray area. To confirm this, the quantity $\langle m(t)\rangle = \frac{1}{t}\sum_{l=1}^{t} m(l)$ is also measured, where $m(l)$ is the observable m observed at time l in the MC simulations. $E(t)$ is defined in the same way. As shown in Figs. 5(c) and 5(d), $m(t)$ and $E(t)$ converge to 0.38013(1) and −0.27634(2), respectively, which are the values of one metastable state.

For a system with size $L \to \infty$, there will be a discontinuity at T_c of order parameter m [44]. For a finite system, the probability $p(m)$ is approximated by two Gaussian curves [45]. As shown in Figs. 5(e) and 5(f), there are clearly double-peak structures at sizes $L = 32$ and 64 in the histograms of m and E. The sharp double peak at $n = 3$ indicates a sufficiently strong first order-transition.

2. n = 2

Theoretically, for a first-order transition, the fitting of Eq. (10) cannot help determine T_c [44]. However, when finite system sizes are small and the temperatures become very close to T_c, Eq. (10) is used here to determine y_t. Figure 6(a) shows the lines Q vs T in the regimes of T_c in the range $5.7502 < T < 5.7532$ with various system sizes $L = 16$–48. By performing the LM algorithm, the values of goodness of fit χ^2/dof, are acceptable and these values are shown in Fig. 6(b). By summing over y_t with different values of $L_{\min}$,

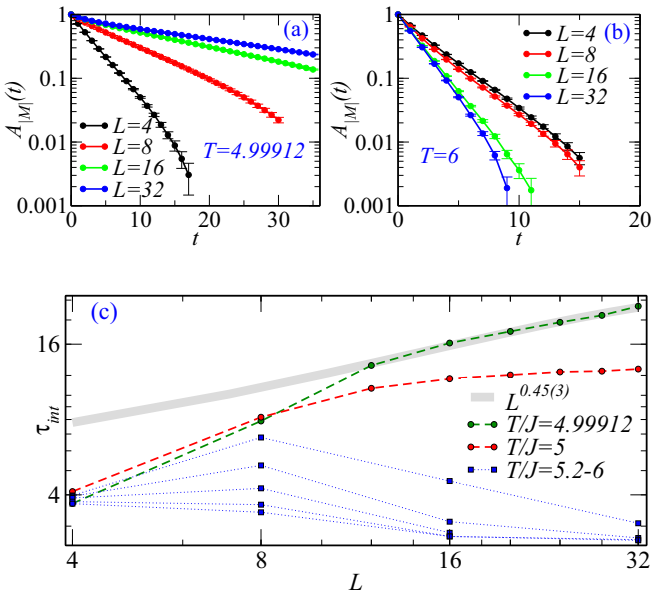

FIG. 7. $A_M(t)$ vs t for $n = 1.5$ CWI model with different sizes at (a) $T = T_c$; (b) $T = 6 > T_c$; (c) $\tau_{\rm int}$ vs L at different temperatures. The exponent z is fitted to be $z = 0.45(3)$.

the average y_t is obtained as 2.95(5) indicating the scaling dimension y_t equals the space dimension d, i.e., $y_t = d$. This result is consistent with the conclusions in Refs. [36–38].

In Figs. 6(c) and 6(d) the double-peak distributions of m and E at $n = 2$ are shown, with different sizes $L = 32, 64, 96$ for $T = 5.755, 5.7518$, and 5.7516. By increasing the system sizes, the peaks become sharper, representing that a first-order transition occurs.

D. $A_M(t)$, $\tau_{\rm int}$ and z at $n = 1.5$

The algorithm has a little critical slowing down. The algorithm we used for $n = 1.5$ is as efficient as the SW algorithm even if we let the clusters be inactive in a probability $1 - 1/n$. This can be judged by the autocorrelation time $\tau_{\rm int}$ and the dynamical exponent z, which can identify the number of MC steps required between two configurations before they can be considered statistically independent [46].

For the absolute magnetism quantity $M = |\mathcal{M}|$, the integrated autocorrelation function $A_M(t)$ is defined as

$$A_M(t) = \frac{\langle M_k M_{k+t}\rangle - \langle M_k\rangle^2}{\langle M_k^2\rangle - \langle M_k\rangle^2}, \tag{15}$$

and the integrated autocorrelation time $\tau_{\rm int}$ is defined as

$$\tau_{\rm int} = \frac{1}{2} + \sum_{t=0}^{\infty} A_M(t). \tag{16}$$

In Figs. 7(a) and 7(b) $A_m(t)$ for the M decays almost purely exponentially in MC time (a linear decay on the linear-log scale). Close to $T_c = 0.499912(5)$, $A_M(t)$ grows with L, while it decreases with L when the temperature deviates away from T_c.

As shown in Fig. 7(c), $\tau_{\rm int}$ behaves like L^z at $T = T_c$ where the dynamical exponent is estimated to be $z = 0.45(3)$ and the error bar in parentheses is the systematic error due to corrections to scaling [47]. This value of z is consistent (within the error bar) with the result $0.443 \pm 0.005 \pm 0.030$ of a "susceptibility-like" observable, or $0.459 \pm 0.005 \pm 0.025$ of an "energy-like" observable from Ref. [47] for the 3D Ising model with the SW algorithm, where the two numbers after the symbol $\pm$ mean two types of error bars.

The correct $\tau_{\rm int}$ and z can be obtained correctly only if one obtains the phase transition points precisely enough. As shown in Fig. 7(c), the values of $\tau_{\rm int}$ at $T/J = 5$ are obviously smaller than those at $T/J = 4.99912$; even the gap between the two temperatures is just 0.00088. Therefore, only the dynamical exponent z at $n = 1.5$ is calculated in this paper.

E. Error bar analysis

The programs are run in 100 threads (bins), and for each thread (bin), a different random number generator seed is used. The first 10^5–10^6 MC steps of simulations are run without measuring any quantities, allowing the systems to reach the stage of equilibrium. Simulation is performed over 10^7 sampling times in the equilibrium states, and the mean values of the quantities are collected from each bin.

For example, the quantity m is averaged from many bins according to $m = \frac{1}{n\text{bin}} \sum_{b=1}^{n\text{bin}} \overline{m}_b$, where $\overline{m}_b$, $b = 1, \cdots, n\text{bin}$ are computed over each bin. The error bar σ is calculated according to

$$\sigma = \sqrt{\frac{1}{n\text{bin}(n\text{bin}-1)} \sum_{b=1}^{n\text{bin}} (\overline{m}_b - m)^2} \tag{17}$$

The quoted error bar corresponds to one standard deviation (i.e., confidence level ≈68%).

The error bars of the fitted exponents are estimated by the diagonal elements of the covariance matrix $[C] = [\alpha]^{-1}$, where α is defined by [35]

$$\alpha_{kl} = \sum_{i=1}^{N} \frac{1}{\sigma_i^2} \left[\frac{\partial Q(T_i; \{a_n\})}{\partial a_k} \frac{\partial Q(T_i; \{a_n\})}{\partial a_l} \right]. \tag{18}$$

V. DISCUSSION AND CONCLUSION

It should be noted that the loop model can be obtained as a high-temperature expansion of various cubic models, such as both face cubic and corner cubic models [4], in which the spins point to the corners of an n-dimensional hypercube, but it also arises as a high-temperature expansion of the $O(n)$ vector spin model in certain settings. The descriptor "cubic" or "$O(n)$" refers to a symmetry of the spin Hamiltonian and has no immediate interpretation in the loop language. Furthermore, the face cubic and corner cubic models can both be related to this same loop model but can have entirely different phase transitions [4].

In conclusion, we have proposed the CWI model, composed of an Ising model with an additional cluster weight in the partition function with respect to the traditional Ising model. In order to simulate the CWI model, we apply an efficient cluster algorithm by combining color assignation and the SW method. The algorithm has almost the same efficiency as

the SW method; i.e., the dynamical exponent for the absolute magnetization $z = 0.45(3)$ at $n = 1.5$ is consistent with that of the standard SW method.

Second-order transitions emerge with $1 \leqslant n < n_{cri}$, and first-order transitions occur when $n \geqslant n_{cri}$ ($n_{cri} \approx 2$) in the CWI model on the 3D lattices, and the universalities of our CWI model and the loop model [21] are completely different. The first-order transition is verified by the signatures of hysteresis, double-peak structure of histograms for the order parameters, and the value of the critical exponent $y_t = d$. Our results can be helpful in the understanding of traditional statistical mechanics models.

ACKNOWLEDGMENTS

We thank Prof. Youjin Deng and the referees for their very valuable suggestions. We also thank T. C. Scott of of RWTH-Aachen University for helping prepare this manuscript. C.D. is supported by the National Science Foundation of China (NSFC) under Grants No. 11975024, No. 11774002, and No. 11804383 and the Anhui Provincial Supporting Program for Excellent Young Talents in Colleges and Universities under Grant No. gxyqZD2019023. W.Z. is supported by the open Project No. KQI201 from Key Laboratory of Quantum Information, University of Science and Technology of China, Chinese Academy of Sciences and by NSFC under Grant No. 51901152.

APPENDIX: $n = 1$ AS TEST EXAMPLE

To verify our method and results, we first simulate the model with $n = 1$ on the 3D lattice equivalent to the 3D Ising model, whose critical point is known at $T_c = 4.5110(3)$ [48]. Our result $T_c = 4.5115(1)$ from the Binder ratio Q according to Eq. (10) is consistent with results in Ref. [48]. Apart from the critical points, y_t and y_m are also very consistent with the results in Ref. [21]. We obtain $y_t = 1.584(4)$, while y_t takes a value of 1.588(2) in Ref. [21].

Figure 8(a) shows the lines Q vs T in the regimes of T_c in the range $4.506 < T < 4.518$ with various system sizes $L = 16$–144. Using the data Q vs T beginning with different values of $L_{\min} = 16, \ldots, 48$ and the fixed maximum size $L_{\max} = 144$, the critical temperature is obtained as $T_c = 4.5115(1)$, which is consistent with a more precise value $1/T_c = 0.221654626(5)$ [34].

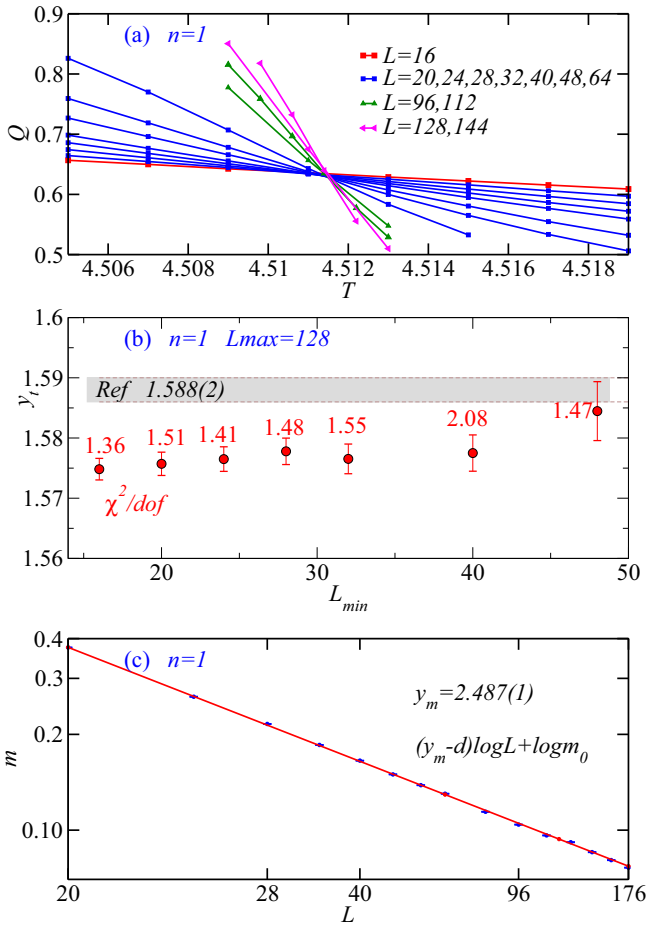

FIG. 8. (a) Binder ratio Q vs T at $n = 1$ with different sizes. The critical point is $T_c = 4.5115(1)$, and $Q_0 = 0.62(4)$. (b) y_t vs $L_{\min}$. The values of χ^2/dof are labeled. (c) The log-log plot of the magnetization m vs L.

In Fig. 8(b) the red symbols y_t are obtained by fitting the terms including one corrected term $f_1 L^{y_1}$. Increasing $L_{\min}$, y_t gradually converges to a value $y_t = 1.584(4)$ consistent with the known result $y_t = 1.588(2)$ [21] within the error bars when $L_{\min} = 48$. The goodness of fit χ^2 per degree is distributed into an acceptable range between 1.36 and 2.08. In Fig. 8(c) the magnetic exponent $y_m = 2.487(1)$ is consistent with the results $y_m = 2.483(3)$ in Ref. [21] according to Eq. (9).

[1] E. Ising, Beitrag zur Theorie des Ferromagnetismus, Z. Phys. **31**, 253 (1925).
[2] H. E. Stanley, Dependence of Critical Properties on Dimensionality of Spins, Phys. Rev. Lett. **20**, 589 (1968).
[3] D. Kim and P. M. Levy, Critical behavior of the cubic model, Phys. Revs. B **12**, 5105 (1975).
[4] B. Nienhuis, E. K. Riedel, and M. Schick, Critical behavior of the n-component cubic model and the Ashkin-Teller fixed line, Phys. Rev. B **27**, 5625 (1983).
[5] K. Nagai, Phase diagrams of the corner cubic Heisenberg model and its site-diluted version on a triangular lattice: Renormalization-group treatment, Phys. Rev. B **31**, 1570 (1985).
[6] E. Domany, D. Mukamel, B. Nienhuis, and A. Schwimmer, Duality relations and equivalences for models with O(N) and cubic symmetry, Nucl. Phys. B **190**, 279 (1981).
[7] W. A. Guo, H. W. J. Blöte, and B. Nienhuis, Phase diagram of a loop on the square lattice, Int. J. Mod. Phys. C **10**, 301 (1999).
[8] A. M. P. Silva, A. M. J. Schakel, and G. L. Vasconcelos, Monte Carlo algorithm for simulating the O(N) loop model on the square lattice, Phys. Rev. E **88**, 021301(R) (2013).
[9] C. X. Ding, X. F. Qian, Y. J. Deng, and H. W. J. Blöte, Geometric properties of two-dimensional O(n) loop configurations, J. Phys. A: Math. Theor. **40**, 3305 (2007).

[10] W. A. Guo, X. F. Qian, H. W. J. Blöte, and F. Y. Wu, Critical line of an n-component cubic model, Phys. Rev. E **73**, 026104 (2006).
[11] C. X. Ding, G. Y. Yao, S. Li, Y. J. Deng, and W. A. Guo, Universal critical properties of the Eulerian bond-cubic model, Chin. Phys. B **20**, 070504 (2011).
[12] C. X. Ding, W. A. Guo, and Y. J. Deng, Ising-like phase transition of an n-component Eulerian face-cubic model, Phys. Rev. E **88**, 052125 (2013).
[13] B. Nienhuis, Exact Critical Point and Critical Exponents of O(n) Models in Two Dimensions, Phys. Rev. Lett. **49**, 1062 (1982).
[14] V. L. Berezinsky, Destruction of long range order in one-dimensional and two-dimensional systems having a continuous symmetry group I. Classical systems, Sov. Phys. JETP **32**, 493 (1971).
[15] J. M. Kosterlitz and D. J. Thouless, Ordering, metastability and phase transitions in two-dimensional systems, J. Phys. C **5**, L124 (1972).
[16] J. M. Kosterlitz, The critical properties of the two-dimensional xy model, J. Phys. C **7**, 1046 (1974).
[17] W. A. Guo, H. W. J. Blöte, and F. Y. Wu, Phase Transition in the $n > 2$ Honeycomb $O(n)$ model, Phys. Rev. Lett. **85**, 3874 (2000).
[18] Z. Fu, W. A. Guo, and H. W. J. Blöte, Ising-like transitions in the O(n) loop model on the square lattice, Phys. Rev. E **87**, 052118 (2013).
[19] H. W. J. Blöte and M. P. Nightingale, The temperature exponent of the n-component cubic model, Physica A **129**, 1 (1984).
[20] C. X. Ding, H. W. J. Blöte, and Y. J. Deng, Emergent O(n) symmetry in a series of 3D Potts models, Phys. Rev. B **94**, 104402 (2016).
[21] Q. Q. Liu, Y. J. Deng, T. M. Garoni, and H. W. J. Blöte, The O(n) loop model on a three-dimensional lattice, Nucl. Phys. B **859**, 107 (2012).
[22] J. M. Carmona, A. Pelissetto, and E. Vicari, N-component Ginzburg-Landau Hamiltonian with cubic anisotropy: A six-loop study, Phys. Rev. B **61**, 15136 (2000).
[23] R. H. Swendsen and J. S. Wang, Nonuniversal Critical Dynamics in Monte Carlo Simulations, Phys. Rev. Lett. **58**, 86 (1987).
[24] Y. J. Deng, T. M. Garoni, W. A. Guo, H. W. J. Blöte, and A. D. Sokal, Cluster Simulations of Loop Models on Two-Dimensional Lattices, Phys. Rev. Lett. **98**, 120601 (2007).
[25] J. Dubail, J. L. Jacobsen, and H. Saleur, Critical exponents of domain walls in the two-dimensional Potts model, J. Phys. A: Math. Theor. **43**, 482002 (2010).
[26] Q. Q. Liu, Y. J. Deng, and T. M. Garoni, Worm Monte Carlo study of the honeycomb-lattice loop model, Nucl. Phys. B **846**, 283 (2011).
[27] Y. D. Xu, Q. Q. Liu, and Y. J. Deng, Monte Carlo study of the universal area distribution of clusters in the honeycomb O(n) loop model, Chin. Phys. B **21**, 070211 (2012).
[28] K. J. Cohn, Cyclomatic numbers of planar graphs, Discrete. Math. **178**, 245 (1998).
[29] G. Bhanot, M. Creutz, and J. Lacki, Low-Temperature Expansion for the Ising Model, Phys. Rev. Lett. **69**, 1841 (1992).
[30] N. Prokof'ev and B. Svistunov, Worm Algorithms for Classical Models, Phys. Rev. Lett. **87**, 160601 (2001).
[31] M. Sweeny, Monte Carlo study of weighted percolation clusters relevant to the Potts models, Phys. Rev. B **27**, 4445 (1983).
[32] E. M. Elçi and M. Weigel, Dynamic connectivity algorithms for Monte Carlo simulations of the random-cluster model, J. Phys. Conf. Ser. **510**, 012013 (2014).
[33] V. K. Gore and M. R. Jerrum, The Swendsen-Wang process does not always mix rapidly, J. Stat. Phys. **97**, 67 (1999).
[34] A. M. Ferrenberg, J. H. Xu, and D. P. Landau, Pushing the limits of Monte Carlo simulations for the three-dimensional Ising model, Phys. Rev E **97**, 043301 (2018).
[35] D. W. Marquardt, An algorithm for least-squares estimation of nonlinear parameters, J. Soc. Ind. Appl. Math. **11**, 431 (1963).
[36] M. E. Fisher and A. N. Berker, Scaling for first-order phase transitions in thermodynamic and finite systems, Phys. Rev. B **26**, 2507 (1982).
[37] K. Vollmayr, J. D. Reger, M. Scheucher, and K. Binder, Finite size effects at thermally-driven first order phase transitions: A phenomenological theory of the order parameter distribution, Z. Phys. B **91**, 113 (1991).
[38] J. Lee and J. M. Kosterlitz, Finite-size scaling and Monte Carlo simulations of first-order phase transitions, Phys. Rev. B **43**, 3265 (1991).
[39] Y. J. Deng, W. A. Guo, J. R. Heringa, H. W. J. Blöte, and B. Nienhuis, Phase transitions in self-dual generalizations of the Baxter-Wu model, Nucl. Phys. B **827**, 406 (2010).
[40] S. S. Wang, W. Z. Zhang, and C. X. Ding, Percolation of the site Random-Cluster model by Monte Carlo method, Phys. Rev. E **92**, 022127 (2015).
[41] W. Z. Zhang, R. X. Yin, and Y. C. Wang, Pair supersolid with atom-pair hopping on the state-dependent triangular lattice, Phys. Rev. B **88**, 174515 (2013).
[42] W. Z. Zhang, R. Li, W. X. Zhang, C. B. Duan, and T. C. Scott, Trimer superfluid induced by photoassociation on the state-dependent optical lattice, Phys. Rev. A **90**, 033622 (2014).
[43] W. Z. Zhang, Y. Yang, L. J. Guo, C. X. Ding, and T. C. Scott, Trimer superfluid and supersolid on two-dimensional optical lattices, Phys. Rev. A **91**, 033613 (2015).
[44] D. P. Landau and K. Binder, *A Guide to Monte Carlo Simulations in Statistical Physics* (Cambridge University Press, Cambridge, 2006).
[45] K. Binder and D. P. Landau, Finite-size scaling at first-order phase transitions, Phys. Rev. B **30**, 1477 (1984).
[46] A. W. Sandvik, Computational studies of quantum spin systems, AIP Conf. Proc. **1297**, 135 (2010).
[47] G. Ossola and A. D. Sokal, Dynamic critical behavior of the Swendsen-Wang algorithm for the three-dimensional Ising model, Nucl. Phys. B **691**, 259 (2004).
[48] K. Binder and E. Luijten, Monte carlo tests of renormalization-group predictions for critical phenomena in Ising models, Phys. Rep. **344**, 179 (2001).